J. Fluid Mech. (1999), *vol.* 379, *pp.* 333–350. Printed in the United Kingdom

The long-time impulse response of compressible swept-wing boundary layers

By M. J. TAYLOR AND N. PEAKE

Department of Applied Mathematics and Theoretical Physics, University of Cambridge, Silver Street, Cambridge CB3 9EW, UK

(Received 13 May 1998 and in revised form 4 September 1998)

Following the investigation of the long-time limit of the impulse response of an incompressible swept boundary layer (Taylor & Peake 1998), we now consider the corresponding behaviour of two representative sets of compressible swept-wing profiles, one set in subsonic flow and the other in supersonic flow. The key feature of the incompressible analysis was the occurrence of modal pinch points in the cross-flow wavenumber plane, and in this paper the existence of such pinches over a wide portion of space in high-speed flow is confirmed. We also show that close to the attachment line, no unstable pinches in the chordwise wavenumber plane can be found for these realistic wing profiles, contrary to predictions made previously for incompressible flow with simple Falker–Skan–Cooke profiles (Lingwood 1997). A method for searching for absolute instabilities is described and applied to the compressible boundary layers, and we are able to confirm that these profiles are not absolutely unstable. The pinch point property of the compressible boundary layers is used here to predict the maximum local growth rate achieved by waves in a wavepacket in any given direction. By determining the direction of maximum amplification, we are able to derive upper bounds on the amplification rate of the wavepacket over the wing, and initial comparison with experimental data shows that the resulting N-factors are more consistent than might be expected from existing conventional methods.

1. Introduction

Following the study of the long-time limit of the causal response of incompressible three-dimensional swept-wedge and swept-wing boundary layer flows to impulsive forcing in Taylor & Peake (1998) (referred to herein as TP), we examine the impulse response of compressible swept-wing boundary layers. Since simple models of swept-wing boundary layers are not available in compressible flow, we will study instead realistic, representative profiles: one (subsonic) set taken from a genuine swept-wing and another (supersonic) set taken from a standard wind-tunnel model. Our aim is to apply the method described in TP to these profiles, and in the subsonic case, to present a new method for predicting the onset of transition.

The properties of pinch points occurring in the wavenumber plane corresponding to the crossflow direction on incompressible swept wedges and wings are discussed in TP. The Falkner–Skan–Cooke (FSC) boundary layer solution, which describes the boundary layer flow over a swept wedge, contains two parameters which can be used to vary the magnitude of the inflectional crossflow velocity component. These are the Hartree pressure gradient parameter and the flow angle. It was found that

crossflow-induced pinch points occurred at a range of pressure gradients, with the minimum flow angle at which a pinch point occurs decreasing as the positive pressure gradient is reduced. The growth rate at a pinch point was destabilized by increasing Reynolds number, and the case of negative pressure gradient was found to be very destabilizing. It was shown that by locating the pinch points in the crossflow-direction, at which the crossflow-direction group velocity component is zero, we can obtain the maximum growth rate obtained by a single wave contained in a wavepacket travelling in the streamwise direction. The boundary layer on a genuine swept airfoil, namely the N416, was also examined and this boundary layer was also shown to support the crossflow-induced pinch point mechanism. The analysis was then extended to search for pinch points in directions other than the crossflow direction, and it was shown that by doing so the maximum growth rate of the travelling wave system, which is found to be purely temporal, can be obtained. In this paper we will examine the boundary layer on a swept wing which is designed for use in the subsonic compressible regime, and locate the local maximum amplification rates of the travelling wave system in order to study the evolution of the wavepackets as we proceed down the wing chord. Also in this paper an analysis of the pinch point properties of the boundary layers on a supersonic airfoil at a range of Mach numbers is performed. In particular we will be examining the possibility of pinch points occurring in the wavenumber plane corresponding to the chordwise direction in the leading-edge region of a genuine swept airfoil, since chordwise pinch points were found at high flow angles in FSC boundary layers by Lingwood (1997). We note also that a recent analysis has been completed by Ryzhov, Cole & Malmath (1998) and Ryzhov & Terent'ev (1998), using rational triple-deck analysis to study viscous instability modes.

In § 2 the subsonic swept-wing boundary layer velocity profiles are described and the theory of the pinch point mechanism is discussed. We analyse one particular subsonic profile in § 3. In § 4 we describe the variation of search direction method and apply it to look for chordwise pinch points in compressible swept-wing boundary layers. In § 5 we discuss the various e^N integration strategies, and carry out an analysis of the evolution of wavepackets on the subsonic swept wing. Results are compared with those found using an envelope e^N method and experimental results. Conclusions are given in § 6.

2. Problem formulation

We use the displacement thickness δ^* as our length scale, and define the Reynolds number as

$$R_{\delta^*} = \frac{U^*_\infty \delta^*}{\nu^*},$$

where U^*_∞ is the local inviscid outer flow. The boundary layer profiles are generated from the pressure distribution using the method of Kaups & Cebeci (1977) who, by limiting their attention to wings of a trapezoidal planform (and ignoring wing twist) and deducing that the absence of pressure gradient along generators is equivalent to the conical flow assumption, wrote the three-dimensional flow equations in a form similar to the two-dimensional flow equations using similarity transforms. They then solved these equations using a finite difference method. In this paper we examine four sets of boundary layer flows with the pressure coefficient curves shown in figure 1. A typical boundary layer profile in case 1, for which the cruise Mach number is 0.743 with a leading edge sweep of 22°, is shown in figure 2, where U and W are

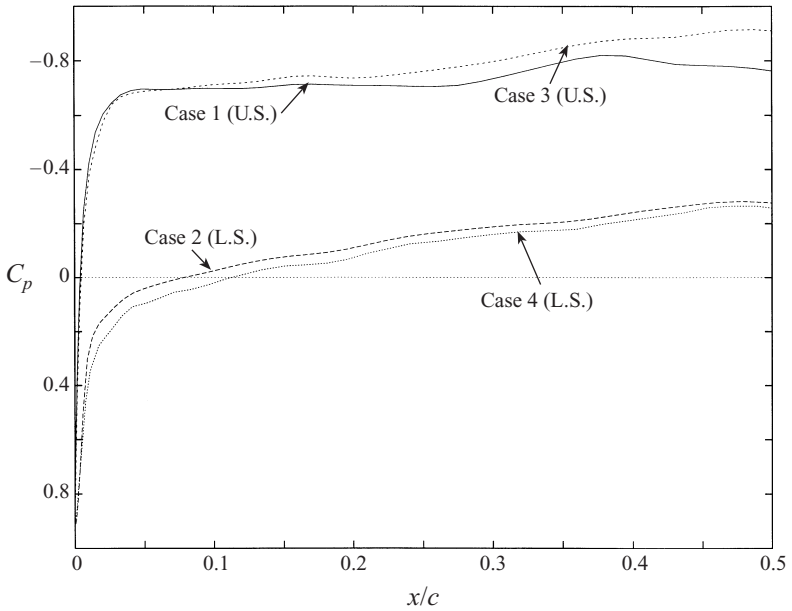

FIGURE 1. Pressure coefficients for four cases on the subsonic swept wing. Cases 1 and 3 are on the upper surface (U.S.), and cases 2 and 4 on the lower surface (L.S.).

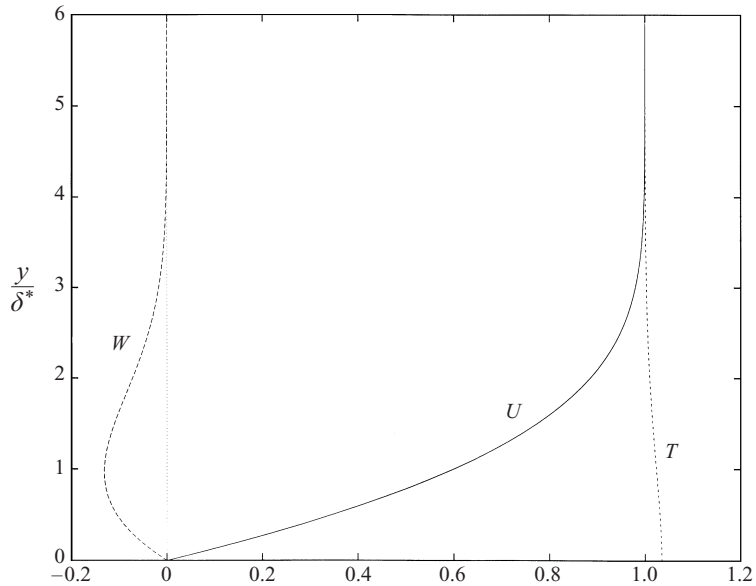

FIGURE 2. Boundary layer profile at point of maximum crossflow level (13%) on the upper surface of the subsonic wing.

the velocity components in the streamwise and crossflow directions respectively and T is the temperature profile. The velocity components are non-dimensionalized with respect to the local inviscid free-stream velocity, while the temperature component is non-dimensionalized with respect to the free-stream temperature. This particular

profile is on the upper surface of the wing and gives the maximum level of crossflow (13%) with a flow angle of 45°, and is located very close to the leading edge.

We derive linear stability equations by assuming that the mean flow is locally parallel, leading to an associated eigenvalue problem of the form

$$D(\alpha, \beta, \omega, R_{\delta^*}) = 0,$$

where α and β are the wavenumbers in the streamwise and crossflow directions respectively, and ω is the complex frequency. These equations are given in Mack (1984) and Malik (1990). The temporal and spatial eigenvalue spectra of the compressible stability problem are found using a global fourth-order finite difference method described in Taylor (1997). We make use of Sutherland's viscosity law

$$\mu^* = \text{const.}\frac{T^{*1.5}}{T^* + T_s^*},$$

where $T_s^* = 110.4$ K, and the thermal conductivity, κ^*, is calculated using the Prandtl number $\sigma^* = 0.72$ and constant specific heat $C_p^* = 0.24$ as

$$\kappa^* = \frac{\sigma^*}{C_p^*}\mu^*.$$

The theory used to obtain the causal solution to the impulse problem in the long-time limit $t \to \infty$ is discussed in detail in TP, so only a brief summary will be given here. We apply Briggs' method to solve the governing equations subject to an impulsive forcing $\delta(x - x_0)\delta(z - z_0)\delta(t)$, and the space–time evolution of the response is then described by a Green's function of the form

$$G(x, z, t) = \frac{1}{8\pi^3}\int_L \mathrm{d}\omega \int_E \int_F \mathrm{d}\alpha\mathrm{d}\beta \frac{\exp[\psi(\alpha, \beta)t]}{D(\alpha, \beta, \omega, R_{\delta^*})}, \tag{2.1}$$

where

$$\psi(\alpha, \beta) \equiv \psi_r + \mathrm{i}\psi_i = \mathrm{i}\left[\alpha\frac{(x - x_0)}{t} + \beta\frac{(z - z_0)}{t} - \omega(\alpha, \beta)\right]. \tag{2.2}$$

The inversion contour L in the complex frequency plane is a horizontal line located above all the singularities of the integrand, while the E and F contours are initially taken along the real α- and β-axes respectively. We perform the ω inversion integral and consider the discrete response only, which is sufficient to determine the long-time limit of the causal solution. This is found using the method of steepest descents to study the asymptotic behaviour of the integral for large t, where $(x - x_0)$ and $(z - z_0)$ are also large parameters and $u \equiv (x - x_0)/t$ and $v \equiv (z - z_0)/t$ are $O(1)$. Dominant contributions are given by the saddle points of $\psi(\alpha, \beta)$, i.e. points where

$$\frac{\partial \omega_r}{\partial \alpha_r} = u, \quad \frac{\partial \omega_r}{\partial \beta_r} = v,$$

$$\frac{\partial \omega_i}{\partial \alpha_r} = 0, \quad \frac{\partial \omega_i}{\partial \beta_r} = 0.$$

The maximum value of the growth rate

$$\psi_r = (\omega_i - \alpha_i u - \beta_i v),$$

denoted ψ_r^{max}, occurs when $\alpha_i = \beta_i = 0$ (figure 3). Pinch points in the β-plane are points where $v = 0$, and in order to find these pinch points we will use the techniques

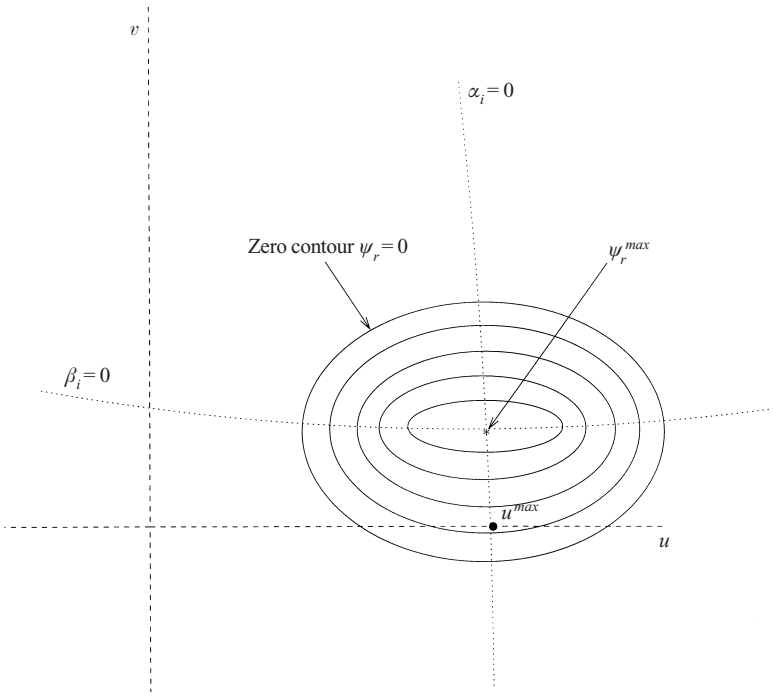

FIGURE 3. Sketch of contours of $\psi_r \geqslant 0$ in the (u, v)-plane.

devised by Briggs (1964), Bers (1975) and Kupfer, Bers & Ram (1987), as described in TP.

3. Crossflow-direction analysis of a single profile

3.1. *Pinch points*

Figure 4 shows the complex ω and β, the crossflow wavenumber, planes at a crossflow-induced pinch point for the boundary layer profile shown in figure 2 at $R_{\delta^*} = 328.9$. The value of α, the wavenumber in the streamwise direction, is purely real ($\alpha = 0.11086$), and was chosen to correspond to the point marked u^{max} on figure 3, where u^{max} is located at the point of maximum temporal growth rate at a crossflow-induced pinch point for this particular profile. At the pinch point the crossflow group velocity component is zero, and the streamwise group velocity component is purely real ($u^{max} = 0.574$) as $\partial\omega_i/\partial\alpha_r = 0$. The mapping of the dashed line L in figure 4(a) into the β-plane in (b) shows the occurrence of this pinch between the two spatial branches 1 and 2. The dotted lines emerging from the pinch point in the β-plane describe how the two pinching modes follow the direction of the arrows into distinct halves of the β-plane as we increase the value of ω_i from its value at the pinch, which is an essential characteristic of a genuine pinch point. Also in figure 4(a) we can observe the mapping of the contour F in the β-plane onto the unstable temporal branch in the ω-plane, which is characterized by a cusp, and the position of the apex of the cusp corresponds to the value of ω at the pinch point. In figure 5 the magnitude of the growth rate at unstable crossflow pinch points is plotted for a range of real values of the streamwise wavenumber α. The point u^{max} is marked on the graph corresponding to the point where $\partial\omega_i/\partial\alpha_r = 0$. It is only this maximum point which corresponds

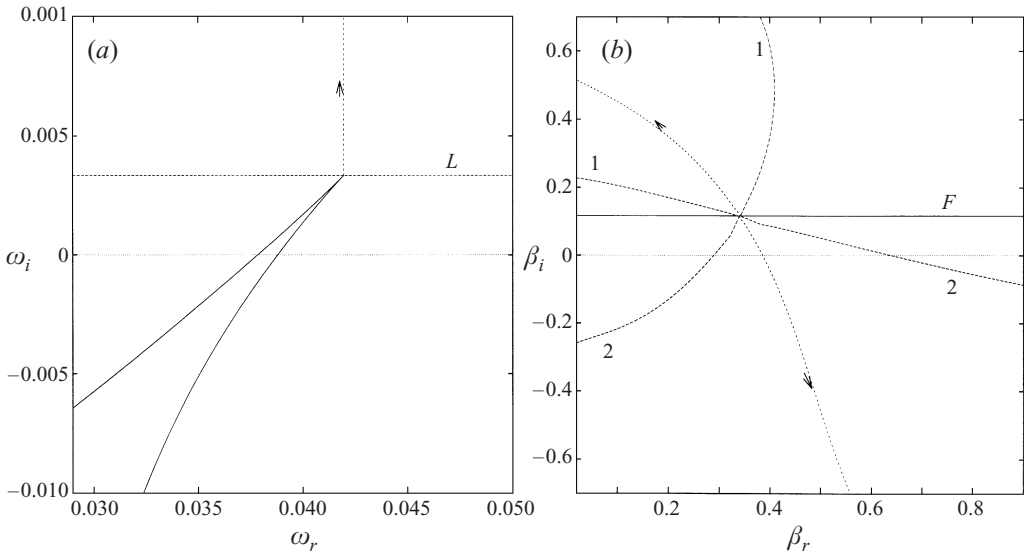

FIGURE 4. Pinch point at u^{max} for the boundary layer profile in figure 2 at $R_{\delta^*} = 328.9$. In (*a*) we show the cusp in the unstable temporal branch in the ω-plane and in (*b*) the pinch occurring between two spatial branches labelled 1 and 2.

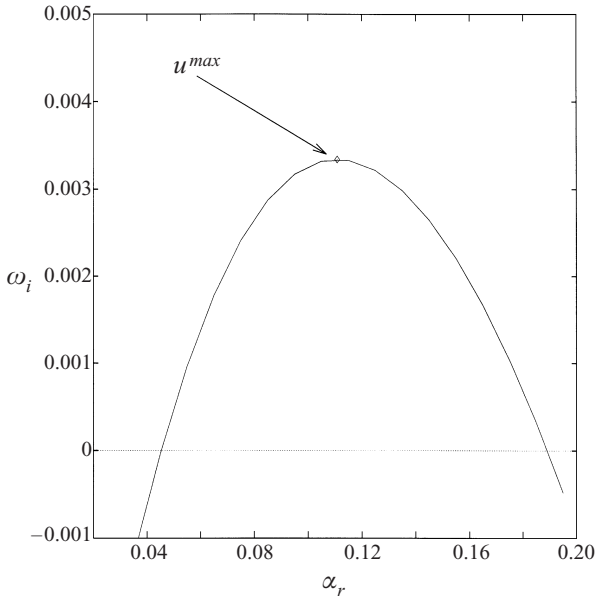

FIGURE 5. Curve of the growth rates at pinch points for the profile given in figure 2 at $R_{\delta^*} = 328.9$ for a range of real streamwise wavenumbers α.

to forcing by the impulse $\delta(x - x_0)\delta(z - z_0)\delta(t)$; other points in fact corrrespond to forcing by $\delta(x - x_0)\exp(\mathrm{i}\alpha_r t)\delta(t)$.

3.2. *Search for absolute instabilities*

A flow that is absolutely unstable supports disturbances that grow in time at a fixed point in space, eventually leading to nonlinearities and thereby causing transition

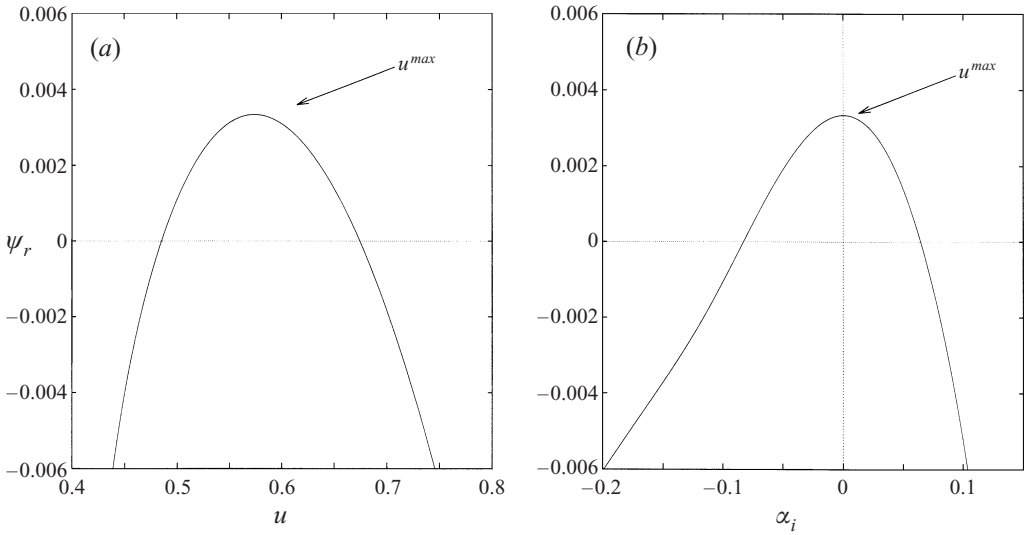

FIGURE 6. Graphs of the growth rate ψ_r for $v = 0$ for (a) varying u and (b) varying α_i for the profile in figure 2 with $R_{\delta^*} = 328.9$.

to turbulence. Brevdo (1991) has shown that it is a requirement for an absolute instability to occur in three dimensions that simultaneous pinch points occur in both wavenumber planes at a positive value of the growth rate ψ_r. At such a simultaneous pinching the group velocity is zero, i.e.

$$\frac{\partial \omega}{\partial \alpha_r} = u = 0, \quad \frac{\partial \omega}{\partial \beta_r} = v = 0.$$

Therefore, in order for an absolute instability to occur, the region enclosed by the zero contour ($\psi_r = 0$) in figure 3 must contain the origin ($u = v = 0$), where $\psi_r = \omega_i$. This is only a necessary condition for the occurrence of an absolute instability, and one would also have to confirm that there was a genuine simultaneous double pinch at the point $u = v = 0$. In order to investigate whether the profile shown in figure 2 at $R_{\delta^*} = 328.9$ can support absolute instabilities, we evaluate the growth rate ψ_r along the u-axis of figure 3. In figure 6(a) u is plotted against ψ_r with $v = 0$. The unstable region ($\psi_r > 0$) lies between $u = 0.486$ and $u = 0.674$ with the maximum value of $\psi_r = 0.003\,34$ occurring at $u^{max} = 0.574$, which shows that this particular profile does not support an absolute instability at this Reynolds number. In figure 6(b) ψ_r is plotted against α_i at $v = 0$ and, as discussed previously, we see that the maximum value of ψ_r (corresponding to the value u^{max}) occurs when $\alpha_i = 0$. Note that reducing the value of α_i decreases the value of u at the saddle point with $v = 0$. We found no absolute instabilities for any subsonic (or supersonic) boundary layer profiles discussed in this paper.

4. Varying search direction

4.1. *Subsonic boundary layers*

The analysis in the previous section was concerned with finding pinch points in the crossflow wavenumber plane. However, we can develop this technique to determine the maximum growth contained in a wavepacket in any given direction, and thereby

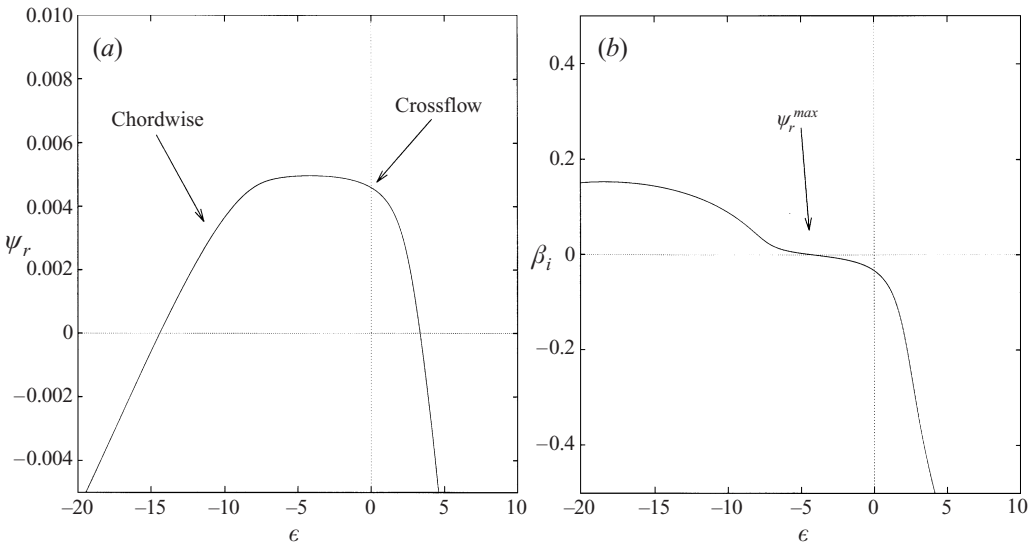

FIGURE 7. (*a*) ϵ against ψ_r and (*b*) ϵ against β_i for the FSC boundary layer with $\beta_H = 1.0$ and $\theta = 79°$.

locate the maximum local growth rate of the travelling wave system. Recalling figure 3, we see that in order to find the maximum value of ψ_r in the (u, v)-plane we should rotate the u- and v-axes until the u-axis goes through the point ψ_r^{max}. In order to do this we resolve the streamwise and crossflow steady velocity components as

$$\tilde{U} = U\cos\epsilon - W\sin\epsilon, \qquad \tilde{W} = U\sin\epsilon + W\cos\epsilon,$$

and then search for pinch points in the new wavenumber plane corresponding to the $\tilde{W}$ component of the resolved velocity profiles.

In order to demonstrate the application of this method we will examine a single incompressible FSC boundary layer. The derivation of the FSC family of swept boundary layer flows, which is described by the flow angle θ and the Hartree pressure gradient β_H, is discussed in TP. We choose the parameters

$$\beta_H = 1.0, \quad \theta = 79°, \quad R_{\delta^*} = 1000,$$

so that both chordwise- and crossflow-induced pinch points are present in a region very close to the attachment line. ($\theta = 90°$ with $\beta_H = 1.0$ is used to represent the flow at the attachment line of a wing.) Figure 7 presents the results of a variation of search direction analysis on this FSC boundary layer profile. The crossflow-induced pinches are discussed in more detail in TP, while the chordwise wavenumber pinches are discussed in detail by Lingwood (1997). The maximum value of the growth rate, $\psi_r^{max} = 0.004\,971$, occurs at $\epsilon = -4.18°$ (where $\beta_i = 0$, see figure 7*b*). The growth rate $\psi_r = 0.002\,977$ at the chordwise pinch ($\epsilon = -11°$) and $\psi_r = 0.004\,596$ at the crossflow pinch ($\epsilon = 0°$). Our result for the chordwise pinch is in agreement with that of Lingwood (1997). The crossflow-induced pinches imply that disturbances are constrained to convect in the streamwise direction, while the chordwise pinch points entertain spanwise convection. However, as can be seen from figure 7(*a*), there are also unstable pinch points present if we continue to search at lower values of ϵ than $-11°$, implying that disturbances are allowed to convect back towards the leading edge. This could be a very dangerous possibility, with disturbances excited

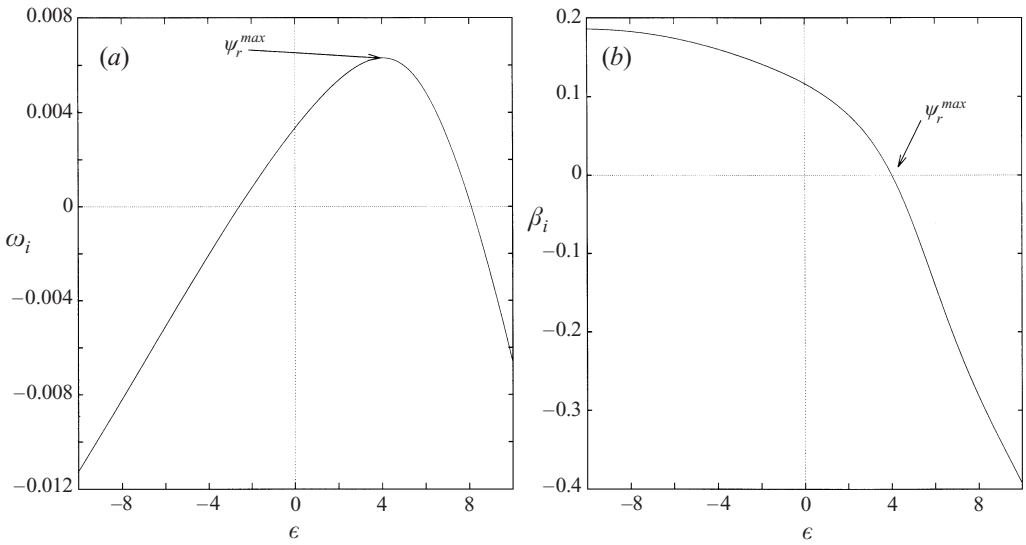

FIGURE 8. (*a*) ϵ against ω_i (= ψ_r as $v = 0$ and $\alpha_i = 0$) at the points $\tilde{u}^{max}$ and (*b*) ϵ against β_i at the points $\tilde{u}^{max}$.

(by an impulse) downstream of the leading edge, propagating toward the leading edge and contaminating the attachment line. Lingwood (1997) suggested that modes propagating along the span may be able to reach nonlinear amplitudes and trigger transition before being convected beyond the wing tip. Gaster (1967), Pfenninger (1965) and Gregory (1960) discuss how if the boundary layer at or near the attachment line is turbulent then the rest of the flow is also expected to be turbulent.

Having shown how our method is applied to the FSC boundary layer, figure 8 now presents the results of a variation of search direction analysis for the compressible subsonic boundary layer shown in figure 2, where the flow angle $\theta = 45^\circ$ and $R_{\delta^*} = 328.9$. The maximum value of ψ_r ($\psi_r = \omega_i$ here as $v = 0$ and $\alpha_i = 0$) in the $\tilde{W}$-direction (i.e. the point $\tilde{u}^{max}$) occurs at $\epsilon = 4^\circ$. There is no chordwise pinch point present in this case, and there are no chordwise pinches present in any of the subsonic boundary layer profiles discussed in this paper. A possible reason for there being no chordwise pinches present in the subsonic case is that the Reynolds numbers are too low to support them. Therefore, in § 4.2 we will examine a swept-wing operating in a supersonic regime in which larger Reynolds numbers are present. In § 5 we will be concerned with determining ψ_r^{max} at each chordwise station as we proceed down the chord of the wing and integrating these values to calculate the amplification of the impulse response in the boundary layer.

4.2. *The impulse response near the leading edge of a swept supersonic airfoil*

The supersonic swept-wing boundary layer analysis is performed using an airfoil designed for wind tunnel experiments at NASA Ames by Radkey, Welge & Felix (1977). The planform is 73.6 cm long and has 30.986 cm maximum span. For the purposes of our work, we chose a spanwise station located at 22.7% of the maximum span, where the leading-edge sweep was 71°, which is close to that envisaged for the next-generation of Supersonic Transport aircraft. The pressure coefficient (C_p) curves, along this spanwise station, are shown for both upper and lower surfaces at two free-stream Mach numbers, $M = 2.003$ and $M = 2.403$, in figure 9. In this paper

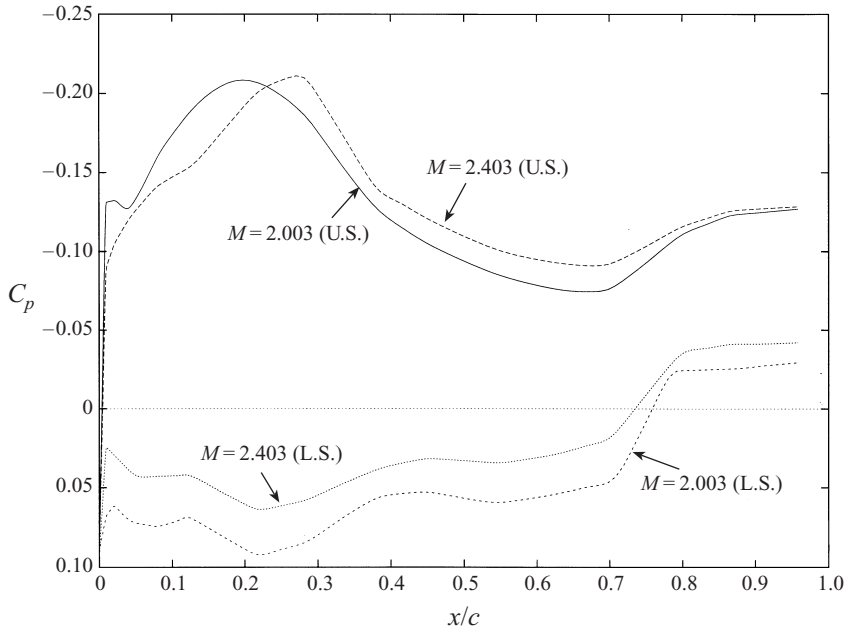

FIGURE 9. Upper (U.S.) and lower (L.S.) surface pressure coefficients for the NASA planform at $M = 2.003$ and $M = 2.403$.

Station	x/c	$\theta^{2.003}$ (deg.)	$R_{\delta^*}^{2.003}$	$\theta^{2.403}$ (deg.)	$R_{\delta^*}^{2.403}$
1	0	90.00	1787.6	90.00	2175.7
2	0.625×10^{-3}	78.54	2625.8	79.08	3231.8
3	0.125×10^{-2}	76.55	3690.0	77.44	4660.2
4	0.1875×10^{-2}	74.82	4209.1	75.98	5340.4

TABLE 1. Table of parameter values for the first four upper surface stations of the Supersonic Transport planform at $M = 2.003$ and $M = 2.403$.

an analysis, at both Mach numbers, of only the upper surface cases is performed. The boundary layer profiles, supplied by BAe Airbus, were generated using these pressure distributions. The chord length at this spanwise station is 51.35 cm. The ambient atmospheric conditions at 55 000 ft (to model the cruise altitude for a supersonic transport) were applied to calculate the free-stream temperature, viscosity and speed of sound, giving Reynolds numbers based on chord $Re_c = 208.7 \times 10^6$ and $Re_c = 250.4 \times 10^6$ for the $M = 2.003$ and $M = 2.403$ cases respectively. Table 1 gives the parameter values for the first four chordwise stations, the boundary layer profiles of which will be used to search for pinch points in the wavenumber plane corresponding to the chordwise direction. For each chordwise station its location (in percentage chord) is given, as well as the flow angle θ and Reynolds number based on displacement thickness R_{δ^*}, with superscripts being used to indicate the Mach number being considered. The values of the flow angles and the Reynolds numbers are both larger in the $M = 2.403$ case. We will also analyse the boundary layer profiles for the $M = 2.003$ case in the incompressible limit, which involves putting $M = 10^{-6}$,

setting the non-dimensional temperature $T = 1.0$ throughout the boundary layer (and putting the derivatives of T equal to zero) and using the same parameter values (flow angle θ and Reynolds number R_{δ^*}) as in the $M = 2.003$ case. As well as looking for chordwise pinch points, a search for genuine absolute instabilities (involving double pinch points) was undertaken at both Mach numbers, but the boundary layers were found to be absolutely stable everywhere. Of course, very near the leading edge our assumption of local parallel flow will not be valid, but the analysis presented here seems appropriate, given that it is seeking to make a comparison with previous work (e.g. Lingwood 1997) based on the same assumption.

Hall, Malik & Poll (1984) demonstrated that the attachment-line boundary layer is susceptible to travelling wave disturbances that propagate along the attachment line, i.e. in the spanwise direction (see also Lin & Malik 1996). It is also shown that these instabilities can be stabilized by the use of suction. In this section we will not be concerned with the behaviour of the attachment-line boundary layer (i.e. station 1), where the existence of spanwise propagating disturbances is well known. Instead the boundary layer in the region close to the attachment line, where the crossflow component of the boundary layer has been established, will be examined for the presence of unstable disturbances being amplified along the span caused by a chordwise pinch. Figures 10(*a*), 10(*b*) and 10(*c*) give the results of the variation of search direction method for stations 2, 3 and 4 respectively. On each graph both Mach numbers (2.003 and 2.403) are shown as well as the incompressible limit of the $M = 2.003$ case (denoted $M = 10^{-6}$), which supports the most unstable growth rates. The two compressible curves ($M = 2.003$ and $M = 2.403$) have very similar shape, but do not support any unstable chordwise pinches as the minimum value of ϵ at which ψ_r is positive is insufficient to reach the chordwise/spanwise orientation. For example, the boundary layer at station 4 at $M = 2.003$, where the flow angle $\theta = 75^\circ$, gives a stable response at $\epsilon = -15^\circ$ and hence no chordwise pinch instability is present. The shape of the left-hand side of the curve for $M = 10^{-6}$ behaves somewhat differently to the compressible curves, extending much further toward the chordwise/spanwise orientation. Although the incompressible curve does not have positive ψ_r at sufficiently low values of ϵ to support unstable chordwise pinch points, it appears from the results that compressibility does have a suppressive effect on chordwise pinch points. Given that the incompressible FSC results at $R_{\delta^*} = 1000$ gave unstable chordwise instabilities, the fact that there are no chordwise pinches in the supersonic airfoil case suggests that the FSC boundary layer may not be an accurate model of the real boundary layer occurring near the leading edge of a swept wing. There are large variations in pressure gradient in this region of the wing, which are not accounted for in the FSC formulation, and these variations must have a significant effect on the characteristics of the long-time impulse response near the leading edge of a genuine swept-wing boundary layer. We therefore reiterate that the realistic boundary layers studied here do not support unstable chordwise pinch points near the attachment line, and that the potential transition mechanism suggested by Lingwood's (1997) FSC analysis, of spanwise convecting disturbances reaching nonlinear amplitudes, does not appear to be present here.

5. Evolution of wavepackets on a swept wing

The e^N method, devised by Smith & Gamberoni (1956) and Van Ingen (1956), assumes that transition starts in the boundary layer of the wing when a small disturbance introduced at the critical Reynolds number has been amplified by a

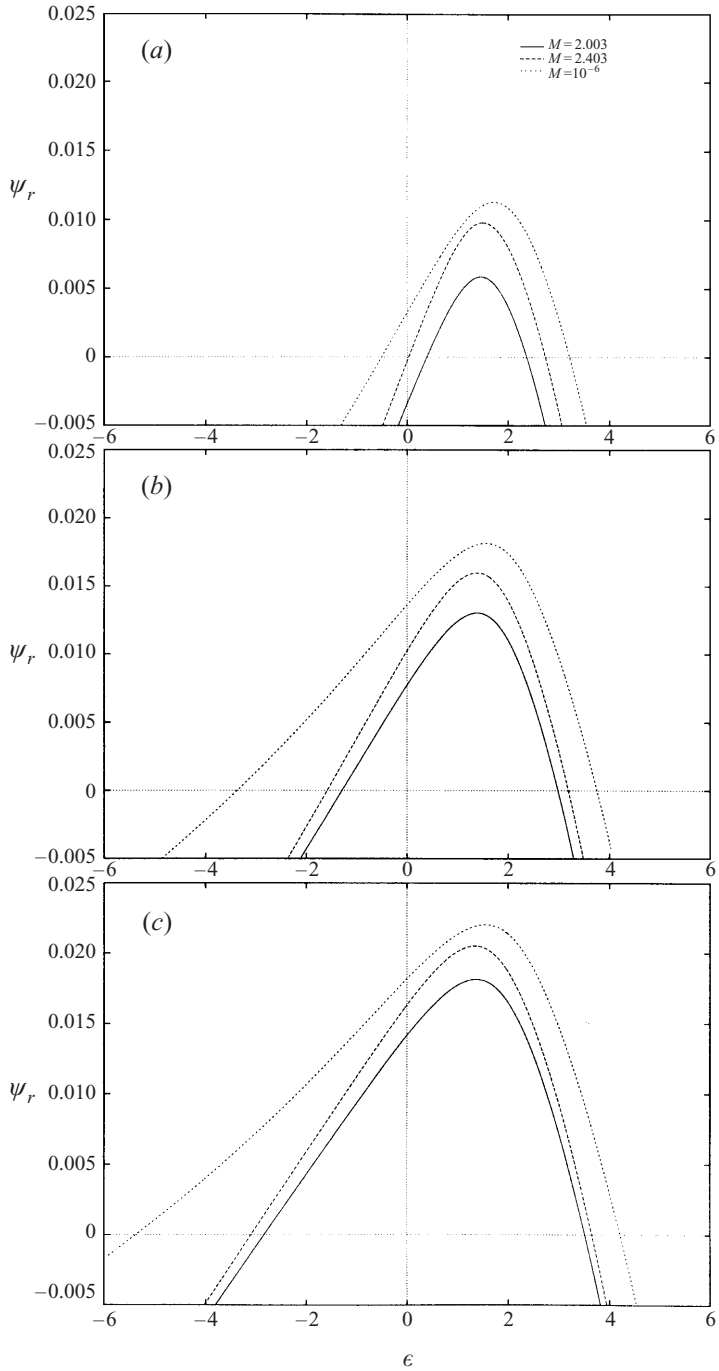

FIGURE 10. Plots of ϵ against ψ_r for stations 2, 3 and 4 in (*a*), (*b*) and (*c*) respectively.

factor e^N, where the value of N is chosen to correlate with experimental results. Although the method uses the parallel flow assumption, Cebeci & Stewartson (1979) point out that the method can still form the basis of a rational attack on the transition prediction problem and is of considerable practical use. It is, however, quite complex

to perform the e^N method on the three-dimensional boundary layer on a swept wing, and numerous strategies for calculating the N-factors have been devised. A conventional e^N analysis involves tracing the evolution of modes of a single frequency along the wing chord using either temporal or spatial temporal linear stability theory. An N-factor may be calculated for temporal stability theory as follows:

$$N = \int_{l_0}^{l} \frac{\omega_i}{|\mathrm{Re}(V_g)|} \mathrm{d}l,$$

where the Gaster (1962) transformation is used to give a growth rate with spatial dimension, l is an appropriate curve along the wing and $\mathrm{Re}(V_g)$ is the real part of the group velocity vector. The dispersion relation provides two real relations among the three complex quantities α, β and ω and in temporal stability theory the spatial wavenumbers α and β are real leaving two arbitrary parameters among α_r, β_r, ω_r and ω_i. This arbitrariness in the choice of the parameters used in computing the N-factors can be removed by numerous approaches. In the envelope method (Malik & Orszag 1980) using temporal theory, the amplification ω_i is maximized at fixed ω_r with respect to the real wavenumbers and the curve l is defined to be everywhere tangent to $\mathrm{Re}(V_g)$. The envelope method can also use spatial amplification theory. Alternatively the constant-β^* method considers waves of fixed ω_r at a range of prescribed real fixed dimensional spanwise wavenumbers, but this approach is only strictly applicable on infinitely long swept wings and so the envelope method is in more general use. Nayfeh (1979) made use of wavepacket theory to remove the arbitrariness in the parameters by prescribing a purely real group velocity vector and examining waves with fixed ω_r and β_r and allowing both spatial wavenumbers to be complex. Malik & Orszag (1980) suggested a variation on this scheme, putting $\omega_i = 0$ and permitting β_r to vary so that the N-factors now depend only on ω_r rather than on both ω_r and β_r as in the case of Nayfeh's formulation, and they demonstrated that the envelope method gave results consistent with the wavepacket approach at considerably less computational expense. All of these methods involve examining the growth of waves of fixed real frequency as they propagate downstream and correlating the resulting N-factor with the location of the onset of transition to turbulence. In this paper, however, we use the pinch point property to evaluate the maximum amplification for any frequency at each station on the wing and integrate these values to calculate an N-factor, which may then be correlated with transition location. This process also offers an insight into the behaviour of wavepackets on a genuine swept wing. In TP we demonstrated that the maximum growth rate of a wavepacket on the swept-wing boundary layer may be calculated using the pinch point property without arbitrarily fixing any of the parameters, and found that the maximum growth rate of the travelling wave system is purely temporal, i.e. $\alpha_i = \beta_i = 0$. We will integrate these growth rates along the wing for each boundary layer profile and calculate N factors for comparison with results from an envelope method and with experimental data.

In order to perform the integration along the wing, the crossflow-induced pinch point u^{max} must be located at each station and then the (u, v)-plane is rotated through an angle ϵ in order to locate the maximum amplification rate in any given direction ψ_r^{max}. These values of ψ_r^{max} are integrated along the wing chord in the group velocity direction in order to calculate an N-factor as

$$N = \int_{\gamma} \frac{\psi_r^{max}}{V_g(s)} \mathrm{d}s, \tag{5.3}$$

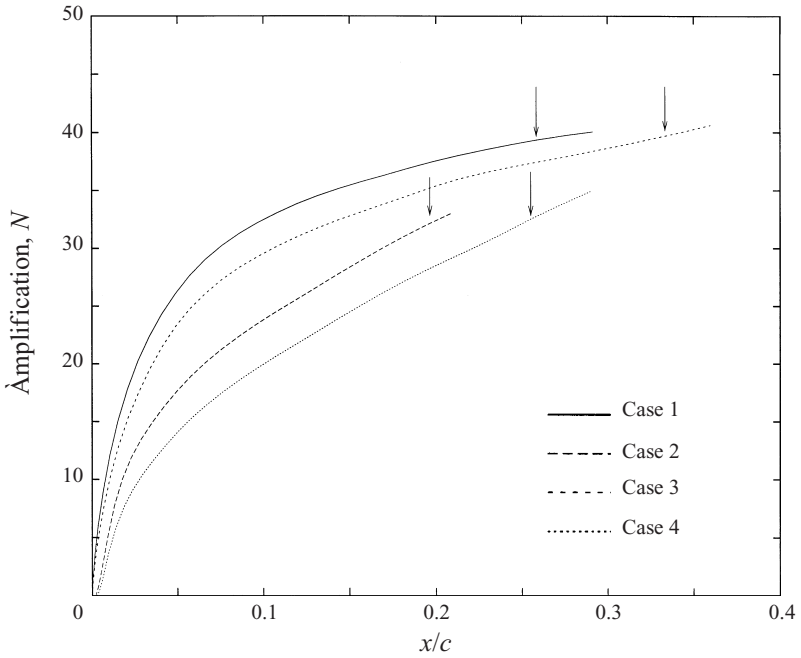

FIGURE 11. The N-factor amplification, calculated using our wavepacket method, for cases 1 to 4 where the arrows mark the location of transition, showing the consistent N-factor achieved by the two TS-dominant cases (1 and 3) and the two CF-dominant cases (2 and 4).

where the path γ is the integral curve in the direction of the group velocity vector V_g of the maximum growth rate. Note that at the points ψ_r^{max} at each station the group velocity has only one real non-zero component because, as discussed in the previous section, the component in the direction of the $\tilde{W}$ velocity component is zero. Upon commencing our analysis of the case 1 upper surface profile (see figure 1) we found that the first station along the wing chord, starting at the leading edge, with a positive ψ_r^{max} (i.e. an unstable response) was station number 3 at 0.045% chord, where the flow angle $\theta = 71^\circ$ and $R_{\delta^*} = 382$. The first two stations (with a higher flow angle and lower R_{δ^*}) were found to give a stable response; station 1 is at 0% chord and station 2 is at 0.02% chord. (A similar result was found for the other cases.) Lingwood (1997) demonstrated the occurrence of unstable pinch points in the chordwise direction near the leading-edge region of a swept wing, with critical Reynolds number 561 at a flow angle of 82°. It is, therefore, not surprising that no unstable pinch points were found at the first two stations from the leading edge of the wing, as the Reynolds number at these stations is well below the critical Reynolds number for such an instability to occur, and so the integration in equation (5.3) is carried out from 0.045% chord down the wing.

In figure 11 the amplification factor N for the case 1 upper surface boundary layer profiles (as well as for three other cases) against percentage chord length found using our wavepacket approach is given. There is strong initial amplification in the first 10% of chord in the region of strong pressure gradient and large levels of crossflow. The rate of increase in the amplification factor N, however, is much reduced in the flat pressure region, eventually reaching a value of 40 at 28% of chord. In figure 12 we plot the values of ϵ through which it was necessary to rotate the (u, v)-plane away from the streamwise/crossflow direction (i.e. the potential flow direction) in

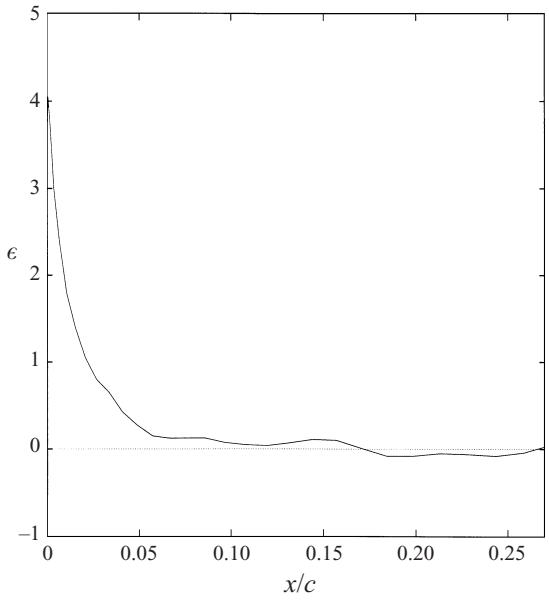

FIGURE 12. The rotation angle ϵ required to locate the maximum amplification factor using our wavepacket approach against percentage chord for the case 1 boundary layer.

order to locate the maximum amplification rate ψ_r^{max} at each chordwise station. In the region of strong favourable pressure gradient and relatively high crossflow levels large values of ϵ were required, while in the flat pressure region the direction of maximum growth is very close to the streamwise direction. This indicates that the amplification in the flat pressure region is caused by the Tollmien–Schlichting (TS) instability of the streamwise profile.

In figure 11 the amplification factor N curve for the case 2 lower surface boundary layer is also shown. There is again strong initial amplification in the very strong favourable pressure gradient region near the leading edge of the wing, but in this case the rate of increase in the factor N remains constant in the region beyond 5% of chord. This is a consequence of the favourable pressure gradient leading to significant crossflow over this region. In experiments performed on this wing, transition to turbulence was found to occur in case 1 (the upper surface boundary layer) at approximately 26% of chord, which corresponds in our wavepacket method to the value $N = 39.5$ from figure 11. The N-factor result for case 1 found using the transition prediction method COSAL Malik & Orszag (1981), which follows the evolution of single temporally unstable modes and calculates the N-factors using the envelope method, gave the value $N = 20.5$ corresponding to the location of the onset of transition. The N-factors generated by our wavepacket method are, of course, significantly larger than those found using COSAL, as at each and every chordwise station we are always integrating over the most amplified frequency. In case 2 (the lower surface boundary layer), transition to turbulence was found to occur in flight tests at approximately 19% of chord, corresponding to a value from our method of $N = 32$ from figure 11. The equivalent COSAL generated N-factor is $N = 17$. The N-factors at the onset of transition given by both methods here are inconsistent between the upper and lower surfaces. It is desirable in a transition prediction method that consistent N-factors are found at the onset of transition, but both methods give

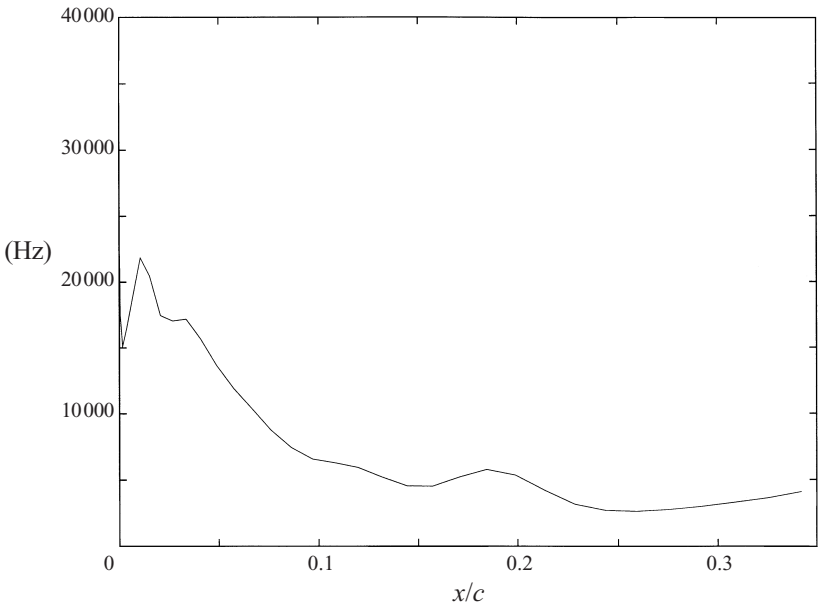

FIGURE 13. Plot of the dimensional frequency at the point of maximum amplification ψ_r^{max} against chord for the case 3 boundary layer.

significantly lower N-factors in the lower surface case than in the upper surface case. However, this is not unexpected as transition is triggered by TS-dominant waves in case 1 (due to the flat pressure region in this case) and by crossflow (CF)-dominant waves in case 2, and indeed the limiting N-factors (i.e. at the onset of transition) are generally different according to whether CF-modes or TS-modes are dominating the instability process (see Schrauf 1994). Schrauf (1994) also found in his analysis of flight experiments with the VFW 614/ATTAS aircraft, that there was a large scatter of limiting N-factors in the TS-dominant cases and consistent limiting N-factors in the CF-dominant cases using the envelope method. This suggests that the envelope method would be of little use in predicting transition triggered by TS waves resulting from a region of flat pressure gradient.

In order to determine whether our wavepacket method can potentially give consistent results for TS-dominant transition as well as CF-dominant transition, we now proceed to examine the cases 3 and 4 sets of boundary layer data. In figure 11 the N-factor curves calculated using our wavepacket method are shown. Experimental data show transition to turbulence occurring at approximately 33% of chord for case 3. Thus the wavepacket method gives a limiting N-factor of 40, which agrees closely with that found using the same method for case 1. Using the COSAL method it was found that the onset of transition occurs at an N-factor of 16 for case 3, which is more than 20% less than the value at transition onset calculated for case 1. In case 4 the transition onset occurs at approximately 25% of chord, giving a limiting N-factor of 32 using the wavepacket method agreeing with the result for case 2. The limiting N-factor for case 4 found using COSAL was 17.5 which is very close to the value found for case 2.

The results from this analysis suggest that our wavepacket approach may be able to provide more consistent N-factors for use in the prediction of TS-dominant transition than the widely utilized envelope method (see figure 11). A much larger

sample of data must be analysed before drawing such a conclusion, but the results here seem promising. In order for a transition prediction scheme to be useful to industry it must provide reliable and consistent limiting N-factors. We suggest that our wavepacket approach, which uses a particular physical property (the pinching mechanism) to calculate the growth rates and does not rely on any arbitrary or intuitive fixing of parameters, may be able to provide a consistent measure of the amount of amplification contained in the swept-wing boundary layer for correlation with the position of the onset of transition. Figure 13 plots the dimensional frequency at the point of maximum amplification found using our wavepacket method against chord for case 3. In the region close to the nose very high frequencies are most unstable, and these could easily be missed in a conventional analysis.

6. Conclusions

In this paper we have applied pinch point theory to swept-wing boundary layers operating in the compressible regime. A method for establishing whether the compressible swept-wing boundary layer supports absolute instabilities is discussed, and no such absolute instabilities were located on the subsonic or the supersonic swept-wing boundary layer. The variation of search direction method is discussed, and it is shown that contrary to predictions made using model FSC profiles, these profiles do not support chordwise pinches, and therefore certainly do not predict that the wavepacket amplifies in the upstream direction. The pinch point property is then used to locate the maximum growth rate obtained by a single wave contained in a wavepacket propagating in the boundary layer. These maximum growth rates are integrated along the wing to calculate N-factors for correlation with transition data. No arbitrary fixing of dispersion relation parameters is required in order to calculate these growth rates, which are found to be purely temporal. Two TS-dominant cases and two CF-dominant cases are examined and the effects of the shape of the pressure coefficient curves on the amplification curve are explored. As expected the limiting N-factors for the TS-dominant cases and the CF-dominant cases differ. However in contrast to the envelope method, which gave a large discrepancy between the limiting N-factors in the two TS-dominant cases, consistent limiting N-factors are found for both the TS- and CF-dominant cases using our wavepacket approach. It is therefore suggested that our wavepacket method may be a more useful design tool. Practical implementation of our scheme would certainly involve a number of computational techniques different to those used in the present study; for instance, one could find the centre of the wavepacket, and hence the maximum growth rate, by maximizing ω_i with α, β real. Validation of our method using further test cases from other aircraft would be invaluable.

M.J.T. acknowledges the support of EPSRC and British Aerospace Airbus Ltd. The authors are very grateful to Dr F Lam for many invaluable discussions and ideas. The authors also thank BAe Airbus Ltd for providing the boundary layer data used in this paper.

REFERENCES

Bers, A. 1975 Linear waves and instabilities In *Physique des Plasmas* (ed. C. DeWitt & J. Peyraud), pp. 113–215. Gordon and Breach.

Brevdo, L. 1991 Three-dimensional absolute and convective instabilities, and spatially amplifying waves in parallel shear flows. *Z. Angew. Math. Phys.* **42**, 911–942.

Briggs, R. 1964 *Electron-Stream Interaction with Plasmas*. MIT Press.

Cebeci, T. & Stewartson, K. 1979 On the prediction of transition in three-dimensional flows. In *Laminar-Turbulent Transition* (ed. R. Eppler & H. Fasel), pp. 243–252. Springer.

Gaster, M. 1962 A note on the relation between temporally-increasing and spatially-increasing disturbances in hydrodynamic stability. *J. Fluid Mech.* **14**, 222–224.

Gaster, M. 1967 On the flow along swept leading edges. *Aeronaut. Q.* **18**, 165–184.

Gregory, N. 1960 Transition and the spread of turbulence on a 60° swept-back wing. *J. R. Aero. Soc.* **64**, 562–564.

Hall, P., Malik, M. & Poll, D. 1984 On the stability of the infinite swept attachment line boundary layer. *Proc. R. Soc. Lond.* A **395**, 229–245.

Kaups, K. & Cebeci, T. 1977 Compressible laminar boundary layers with suction on swept and tapered wings. *J. Aircraft* **14**, 661–667.

Kupfer, K., Bers, A. & Ram, A. 1987 The cusp map in the complex-frequency plane for absolute instabilities. *Phys. Fluids* **30**, 3075–3082.

Lin, R. & Malik, M. 1996 On the stability of attachment-line boundary layers. Part 1. The incompressible swept Hiemenz flow. *J. Fluid Mech.* **311**, 239–255.

Lingwood, R. 1997 On the impulse response for swept boundary layer flows. *J. Fluid Mech.* **344**, 317–334.

Mack, L. 1984 Special course on stability and transition of laminar flow. *AGARD Rep.* 709. NATO.

Malik, M. 1990 Numerical methods for hypersonic boundary layer stability. *Comput. Phys.* **86**, 376–413.

Malik, M. & Orszag, S. 1980 Comparison of methods for prediction of transition by stability analysis. *AIAA J.* **18** 1485–1489.

Malik, M. & Orszag, S. 1981 Efficient computation of the stability of three-dimensional compressible boundary layers. *AIAA Paper* 81–1277.

Nayfeh, A. 1979 Stability of three-dimensional boundary layers. *AIAA Paper* 79–0262.

Pfenninger, W. 1965 Flow phenomena at the leading edge of swept wings. *AGARDograph* 97 Part IV A1. NATO.

Radkey, R., Welge, H. & Felix, J. 1977 Aerodynamic characteristics of a Mach 2.2 advanced supersonic cruise aircraft configuration at Mach numbers from 0.5 to 2.4. Contractors Report CR-145094. NASA.

Ryzhov, O. S., Cole, J. D. & Malmath, N. D. 1998 Excitation of convectively and absolutely unstable disturbances in three-dimensional boundary layers. *AIAA Paper* 98–2861.

Ryzhov, O. S. & Terent'ev, E. D. 1998 Streamwise absolute instability of a three-dimensional boundary layer at high Reynolds number. *J. Fluid Mech.* **373**, 111–153.

Schrauf, G. 1994 Transition prediction using different linear stability analysis strategies. *AIAA Paper* 94–1848.

Smith, A. & Gamberoni, N. 1956 Transition, pressure gradient and stability theory. *Rep.* ES 26388. Douglas Aircraft Co.

Taylor, M. 1997 The stability of the boundary layer on swept wings. PhD thesis, University of Cambridge.

Taylor, M. & Peake, N. 1998 The long-time behaviour of incompressible swept wing boundary layers subject to impulsive forcing, *J. Fluid Mech.* **355**, 359–381 (referred to herein as TP).

Van Ingen, J. 1956 A suggested semi-empirical method for the calculation of the boundary layer transition region. *Rep.* VTH-74. Univ. of Tech, Delft.